



HAL
open science

Determination of single-crystal elasticity constants of the beta phase in a multiphase tungsten thin film using impulse excitation technique, X-ray diffraction and micro-mechanical modeling

Mohamed Fares Slim, Akram Alhussein, Elia Zgheib, Manuel François

► To cite this version:

Mohamed Fares Slim, Akram Alhussein, Elia Zgheib, Manuel François. Determination of single-crystal elasticity constants of the beta phase in a multiphase tungsten thin film using impulse excitation technique, X-ray diffraction and micro-mechanical modeling. *Acta Materialia*, 2019, 175, pp.348-360. 10.1016/j.actamat.2019.06.035 . hal-02276760

HAL Id: hal-02276760

<https://utt.hal.science/hal-02276760>

Submitted on 25 Oct 2021

HAL is a multi-disciplinary open access archive for the deposit and dissemination of scientific research documents, whether they are published or not. The documents may come from teaching and research institutions in France or abroad, or from public or private research centers.

L'archive ouverte pluridisciplinaire **HAL**, est destinée au dépôt et à la diffusion de documents scientifiques de niveau recherche, publiés ou non, émanant des établissements d'enseignement et de recherche français ou étrangers, des laboratoires publics ou privés.



Distributed under a Creative Commons Attribution - NonCommercial 4.0 International License

Note: the changes made in the text are colored in green

Determination of single-crystal elasticity constants of the beta phase in a multiphase tungsten thin film using impulse excitation technique, X-ray diffraction and micro-mechanical modeling

Mohamed Fares Slim ^{a,b*}, Akram Alhussein ^b, Elia Zgheib ^b, Manuel François ^a

^a ICD-LASMIS, Université de Technologie de Troyes, UMR 6281, CNRS, 12 rue Marie Curie, CS 42060, 10004 Troyes, France.

^b ICD-LASMIS, Université de Technologie de Troyes, UMR 6281, CNRS, Antenne de Nogent, Pôle Technologique de Sud-Champagne, 52800 Nogent, France.

*Corresponding author: Mohamed Fares Slim, mohamedfaresslim@gmail.com

Abstract

The scope of this work is to propose a methodology allowing the determination of the single-crystal elasticity constants of a phase included in a multiphase thin film taking into account its microstructure (crystallographic and morphological texture, porosity and multiphase aspect). The methodology is based on the use of a macro-mechanical test, the impulse excitation technique, a micro-mechanical test, X-ray diffraction and the Kröner-Eshelby scale transition model. As a supporting example, it was applied to determine the single-crystal elasticity constants of the W_β tungsten metastable phase embedded in a two phases ($\alpha+\beta$) tungsten thin film deposited on a steel substrate by DC magnetron sputtering. The effects of the grain-shape, the crystallographic texture, the porosity and the W_β volume fraction on the macroscopic elasticity constants were studied. Among all these effects, it was found that the effect of the W_β volume fraction was the most pronounced. The effects of the crystallographic and morphological texture on the microscopic elastic behavior of the film were evaluated. No dominance of the crystallographic or morphological texture effect was observed and their contributions depend on the crystallographic plane and the measurement direction.

Keywords: coating, elastic properties, microstructure, micromechanical modeling, X-ray diffraction.

1. Introduction

The prediction of the elastic behavior of coated components requires a perfect knowledge of the elasticity constants of the coating which depends on its microstructural properties. Generally, thin films are multiphase, textured, porous and present grains with columnar morphology. Thus, knowing only their macroscopic elasticity constants is not sufficient to describe their elastic response. We can cite as example the problem of the determination of the residual stresses issued from the process which requires the knowledge of the single-crystal elasticity constants (SCECs) of the different phases (X-ray Elasticity Constants or Diffraction Stress Factors [1]).

The SCECs can be determined experimentally, directly on single crystal specimens [2-5] or indirectly on macroscopic scale polycrystalline specimens. The second one can use either measurements of the microscopic strain response by diffraction under an applied loading [6-14] or measurements by means of resonant ultrasound spectroscopy (RUS) combined with electromagnetic acoustic resonance (EMAR) and the crystallographic orientations [15-18]. These two approaches combine experimental measurements with theoretical models as micro-mechanical models or finite element models.

In this work, we focus on X-ray diffraction of a composite (film+substrate) sample under applied loading. As a selective method, diffraction allows to probe the microscopic elastic response of a phase within a multiphase film. Using X-ray diffraction, SCECs can be determined from the macroscopic stiffness and the X-ray elasticity constants of the analyzed polycrystal [19]. This procedure is straightforward to use for macroscopically isotropic materials. It was initially introduced by Hauk and Kockelmann [19] for single-phase polycrystals. Then, it was used by different authors to extract the SCECs of single-phase materials with different crystal structures [8, 9, 11, 12, 20]. The main drawback of this method is that the material must follow reasonably the assumptions of $\sin^2\Psi$ method, i.e. the material is macroscopically isotropic. Later on, this methodology was extended to two-phases polycrystals by Fréour et al [6] and used to determine the SCECs of the metastable titanium β phase embedded in a two-phases ($\alpha+\beta$) titanium polycrystal.

In the presence of texture, the use of the X-ray elasticity constants dependent only on the $\{hkl\}$ reflections is no longer possible to relate the macroscopic and the microscopic stress states. However the general X-ray stress factors (also called Diffraction Stress Factors or Generalized Diffraction Elasticity Constants) computed from the Orientation Distribution Function (ODF) is needed. The crystallite group method can also be used [1, 21, 22].

Recently, Faurie et al [7, 23] have determined the SCECs of a {111} fiber textured single-phase gold film. In their first work, Faurie et al [7] have performed strain measurements using X-ray diffraction measurements by means of a four-circle goniometer on the H10 beam line at the French synchrotron radiation facility LURE (Orsay) under imposed in situ tensile loading. Finally, in order to determine the SCECs of the monophasic gold film, they have fitted the experimental data using a least-squares process to a Neerfeld-Hill analytical expression (micro-mechanical model) derived in a previous work [24]. To relate the macro and the micro scales, thanks to the sharp texture of the film, the authors have used the crystallite group method, which leads to simple mathematical expressions. More recently, they have determined the SCECs of a {111} fiber textured single-phase gold film also by using X-ray diffraction under imposed tensile loading. However, in order to extract the SCECs of the thin film, the micro-mechanical self-consistent model was used to fit the experimental data using a least-squares process [23]. As in the previous work they have used the crystallite group method in the micro-mechanical modeling. However, to our knowledge no previous research have treated a multiphase thin film and taken into account the porosity, the crystallographic texture, the morphological texture and the multiphase aspect.

The goal of this work is to propose a methodology to extract the SCECs of a phase included in a multiphase thin film taking into account its microstructural properties (presence of different phases, presence of porosity, crystallographic texture and morphological texture). The basic idea of the methodology developed in this work is to use a macro-mechanical test, the impulse excitation technique (IET), which allows to measure some components of the anisotropic macroscopic elasticity constants and a micro-mechanical test sensitive to crystalline anisotropy, X-ray diffraction under imposed loading, which allows to measure the lattice strains of the probed phase. Finally, the macroscopic and microscopic experimental data will be fitted using the micro-mechanical self-consistent model in order to extract the SCECs. A schematic presentation of the methodology is presented in Fig. 1.

In the present paper, a two-phase tungsten film ($W_{\alpha}+W_{\beta}$) was deposited by DC magnetron sputtering and the cubic A15 (Pm-3n) metastable W_{β} SCECs were determined for the first time using the developed methodology. The microstructure of the deposited film was analyzed using X-ray diffraction and scanning electron microscope. The crystallographic texture, the morphological texture, the porosity and the multiphase aspect were taken into account in the mechanical modeling. The effects of the crystallographic texture, the porosity,

the W_β volume fraction and the morphological texture on the macroscopic and the microscopic elastic behavior of the film were studied.

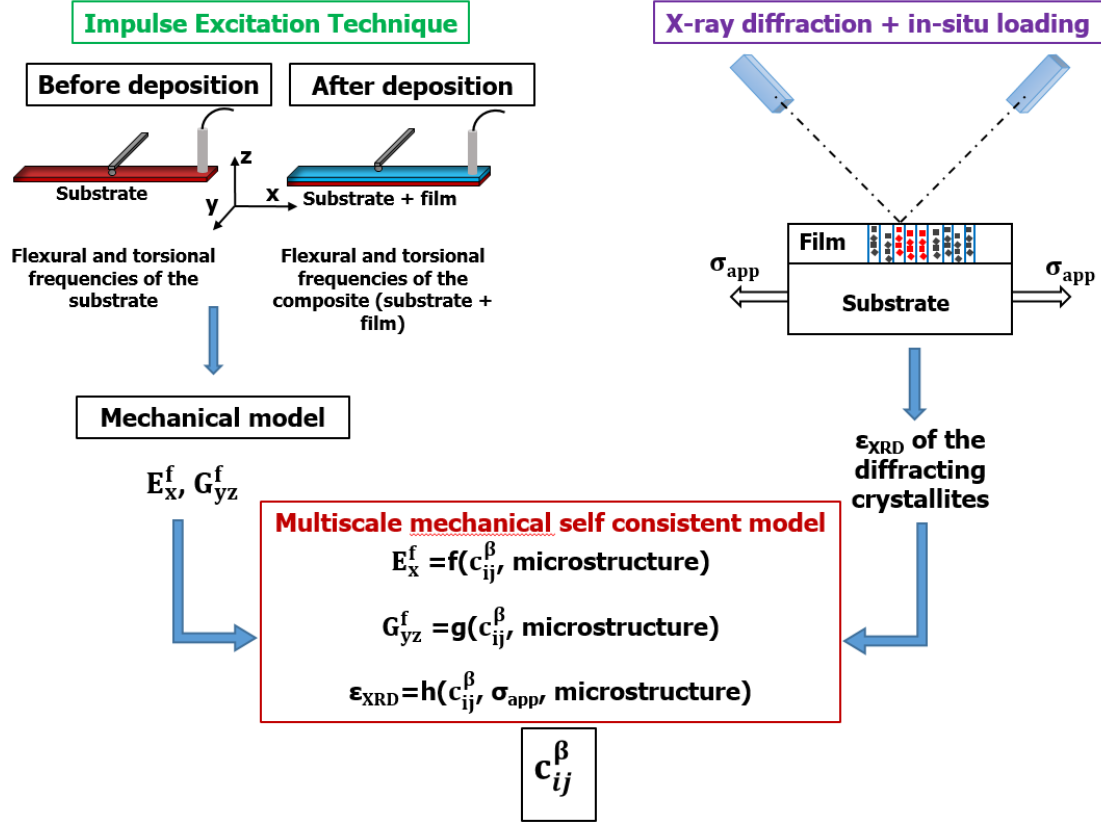


Fig. 1. Schematic representation of the methodology used in the determination of the single-crystal elasticity constants.

2. Theoretical background

2.1. Single-crystal elasticity constants determination

Depending on the crystal structure of a phase, its single-crystal elasticity tensor can be described using a number of independent constants. For example, the single-crystal elasticity tensor of a cubic phase can be described using three independent constants (c_{11} , c_{12} , c_{44}). To determine these constants through an inverse procedure, at least as many independent experimental quantities are required.

In our case, two macroscopic elasticity constants (E_x and G_{yz}) are determined using IET and expressed using the Kröner-Eshelby (KE) self-consistent micro-mechanical model as a function of single-crystal stiffness tensor. Then, the microscopic elastic response of several $\{hkl\}$ planes under imposed loading is probed using X-ray diffraction (XRD) and also expressed using the KE model. Finally, the SCECs will be calculated by minimizing an

objective function defined as the difference between the experimental and the calculated quantities.

Micromechanical models used for elasticity can be classified on two groups, interaction models in which the grain shape is not defined and interaction models where grain shape is defined through a 4th rank tensor or through assumptions on the mechanical state of a film. As examples of the first group are Voigt, Reuss and the Hill models. This type of models is not really adapted for thin films which generally present a grain shape texture (needle-like grains) [25]. However, as examples of direction-dependent grain-interaction models are the Kröner-Eshelby model, the Vook-Witt and the inverse Vook-Witt models. It was demonstrated by Welzel et al [26, 27] that similarities between the Vook-Witt and the Kröner-Eshelby models occur for a polycrystal with extreme flat disc-shaped grains. Such similarities between the inverse Vook-Witt and the Kröner-Eshelby models occur also but much less in the case of extreme needle-like grains. Hence, the Kröner-Eshelby model will be used in this work. Furthermore, the Kröner-Eshelby model will allow the quantification of the grains shape effect on the macroscopic elasticity constants and on the elastic behavior of the diffracting volume.

2.2. *Micro-mechanical Kröner-Eshelby self-consistent model*

The KE model [28, 29] is one of the most commonly used multiscale transition model to describe the elasticity of materials. It relates the macroscopic mechanical state, denoted by $\boldsymbol{\sigma}$ and $\boldsymbol{\varepsilon}$, with the microscopic mechanical state, denoted by $\boldsymbol{\sigma}_\Omega^i$ and $\boldsymbol{\varepsilon}_\Omega^i$, using a polarization tensor.

$$\boldsymbol{\varepsilon}_\Omega^i = (\mathbf{I} + \mathbf{u}_\Omega^i) : \boldsymbol{\varepsilon} = \mathbf{A}_\Omega^i : \boldsymbol{\varepsilon} \quad 1$$

$$\boldsymbol{\sigma}_\Omega^i = (\mathbf{I} + \mathbf{t}_\Omega^i) : \boldsymbol{\sigma} = \mathbf{B}_\Omega^i : \boldsymbol{\sigma} \quad 2$$

\mathbf{t}_Ω^i and \mathbf{u}_Ω^i are 4th rank tensors called polarization tensors. Subscript Ω corresponds to the orientation of the crystallite and superscript i corresponds to the considered phase. In this study, the macroscopic scale corresponds to the thin film and the microscopic scale corresponds to the crystallites. \mathbf{A}_Ω^i and \mathbf{B}_Ω^i are 4th rank tensors called respectively the strain localization tensor and the stress concentration tensor. \mathbf{I} is the 4th rank identity tensor. The use of this model implies that the stress/strain field is considered homogeneous in a representative volume element (RVE) of the film, and also homogeneous in a crystallite. This latter has been

demonstrated by Eshelby in the case of linear elasticity for an ellipsoidal heterogeneity embedded in an infinite matrix [29].

Assuming that crystallites can be represented by ellipsoids, the strain localization tensor \mathbf{A}_Ω^i can be expressed by Eq. 3:

$$\mathbf{A}_\Omega^i = [\mathbf{P}(\mathbf{C}):(\mathbf{c}_\Omega^i - \mathbf{C}) + \mathbf{I}]^{-1} \quad 3$$

$\mathbf{P}(\mathbf{C})$ is a non-symmetric fourth order tensor, called Morris tensor [30] expressed by Eq. 4. It depends on the morphology of the inclusion and the rigidity tensor of the polycrystal.

$$P_{ijkl} = \frac{1}{4\pi} \int_0^\pi \sin \theta \, d\theta \int_0^{2\pi} \gamma_{ijkl} \, d\phi \quad 4$$

With:

$$\gamma_{ijkl} = K_{ij}^{-1}(\xi) \xi_k \xi_l \quad 5$$

$$K_{ip}(\xi) = \mathbf{C}_{ijpl} \xi_j \xi_l \quad 6$$

$$\xi_1 = \frac{\sin \theta \cos \phi}{a_1} \quad \xi_2 = \frac{\sin \theta \sin \phi}{a_2} \quad \xi_3 = \frac{\cos \theta}{a_3} \quad 7$$

$0 < \theta < \pi$ et $0 < \phi < 2\pi$ are spherical coordinates that define the direction of the vector ξ with respect to the principal axes of the ellipsoid, of length $2a_1$, $2a_2$ and $2a_3$ [31]. The morphological texture can be described using the ratios introduced in Eq. 7.

Eq. 1 can be rewritten as following:

$$\boldsymbol{\varepsilon}_\Omega^i = [\mathbf{P}(\mathbf{C}):(\mathbf{c}_\Omega^i - \mathbf{C}) + \mathbf{I}]^{-1} : \boldsymbol{\varepsilon} = [\mathbf{P}(\mathbf{C}):(\mathbf{c}_\Omega^i - \mathbf{C}) + \mathbf{I}]^{-1} : \mathbf{C}^{-1} : \boldsymbol{\sigma} \quad 8$$

The elastic behavior of the polycrystal and of a crystallite are expressed by Eqs. 9 and 10:

$$\boldsymbol{\sigma} = \mathbf{C} : \boldsymbol{\varepsilon} \quad 9$$

$$\boldsymbol{\sigma}_\Omega^i = \mathbf{c}_\Omega^i : \boldsymbol{\varepsilon}_\Omega^i \quad 10$$

The average elastic behavior of a two-phase ($\alpha+\beta$) polycrystal is expressed by Eqs. 11 and 12:

$$\boldsymbol{\sigma} = V_{\alpha}\langle\boldsymbol{\sigma}_{\Omega}^{\alpha}\rangle_{\Omega\in\alpha} + V_{\beta}\langle\boldsymbol{\sigma}_{\Omega}^{\beta}\rangle_{\Omega\in\beta} \quad 11$$

$$\boldsymbol{\varepsilon} = V_{\alpha}\langle\boldsymbol{\varepsilon}_{\Omega}^{\alpha}\rangle_{\Omega\in\alpha} + V_{\beta}\langle\boldsymbol{\varepsilon}_{\Omega}^{\beta}\rangle_{\Omega\in\beta} \quad 12$$

$\langle \ \rangle_{\Omega\in i}$ corresponds to the average of the quantity on all the orientations of phase i . V_i is the volume fraction of phase i .

By substituting Eqs. 8 and 12 in Eq. 9, we find:

$$\boldsymbol{\sigma} = \left[V_{\alpha}\langle\mathbf{c}_{\Omega}^{\alpha} : [\mathbf{P} : (\mathbf{c}_{\Omega}^{\alpha} - \mathbf{C}) + \mathbf{I}]^{-1}\rangle_{\Omega\in\alpha} + V_{\beta}\langle\mathbf{c}_{\Omega}^{\beta} : [\mathbf{P} : (\mathbf{c}_{\Omega}^{\beta} - \mathbf{C}) + \mathbf{I}]^{-1}\rangle_{\Omega\in\beta} \right] : \boldsymbol{\varepsilon} \quad 13$$

Through identification with Eq. 9, the macroscopic rigidity tensor of the two-phase polycrystal is expressed by Eq. 14:

$$\mathbf{C} = \left[V_{\alpha}\langle\mathbf{c}_{\Omega}^{\alpha} : [\mathbf{P} : (\mathbf{c}_{\Omega}^{\alpha} - \mathbf{C}) + \mathbf{I}]^{-1}\rangle_{\Omega\in\alpha} + V_{\beta}\langle\mathbf{c}_{\Omega}^{\beta} : [\mathbf{P} : (\mathbf{c}_{\Omega}^{\beta} - \mathbf{C}) + \mathbf{I}]^{-1}\rangle_{\Omega\in\beta} \right] \quad 14$$

This equation gives the macroscopic elasticity constants of the film E_x and G_{yz} as a function of the single-crystal elasticity constants. The tensor \mathbf{P} is known from the shape of the crystallites and the volume fractions are calculated from X-ray diffraction patterns. It can be noted here that tensor \mathbf{C} is anisotropic due to the shape of the inclusions and to the averaging on the orientations Ω describing the crystallographic texture of the film.

The strain of a crystallite belonging to phase i is expressed by Eq. 8. Using X-ray diffraction, a diffracting volume (DV) is analyzed. The strain measured by X-ray diffraction is the average of all strains of crystallites belonging to the diffracting volume (Fig. 2). Thus, the strain measured by X-ray diffraction is also expressed using the KE model by Eq. 15:

$$\varepsilon_{\phi\Psi}^{\{hkl\}_i} = \ln\left(\frac{\sin\theta_0^{\{hkl\}_i}}{\sin\theta_{\phi\Psi}^{\{hkl\}_i}}\right) = \vec{n} \cdot \langle\boldsymbol{\varepsilon}_{\Omega}^i\rangle_{\Omega\in DV} \cdot \vec{n} \quad 15$$

With $\theta_0^{\{hkl\}_i}$ and $\theta_{\phi\Psi}^{\{hkl\}_i}$ are respectively the position of the diffraction peaks of a non-stressed and of a stressed material.

By substituting Eq. 8 in Eq. 15, we obtain the strain measured by X-ray diffraction:

$$\varepsilon_{\phi\Psi}^{\{hkl\}i} = \vec{n} \cdot \left[\langle [\mathbf{P}: (\mathbf{c}_{\Omega}^i - \mathbf{C}) + \mathbf{I}]^{-1} \rangle_{\Omega \in DV} : \mathbf{C}^{-1} : \boldsymbol{\sigma} \right] \cdot \vec{n} \quad 16$$

With h, k, l the Miller indices, ϕ the azimuth angle, Ψ the tilt angle and \vec{n} the scattering vector defining the measurement direction (Eq. 17, Fig. 3). More details about the geometry of X-ray stress analysis can be found in the literature [32]. Eq. 16 gives the additional equations of Fig. 1: $\boldsymbol{\sigma}$ tensor is a known applied stress and, as before, \mathbf{P} and \mathbf{C} tensors are known. For each selected (ϕ, ψ) couple and diffraction peak $\{hkl\}$ of the investigated phase, an additional equation is obtained.

$$\vec{n} = \begin{pmatrix} \cos \phi \sin \Psi \\ \sin \phi \sin \Psi \\ \cos \Psi \end{pmatrix} \quad 17$$

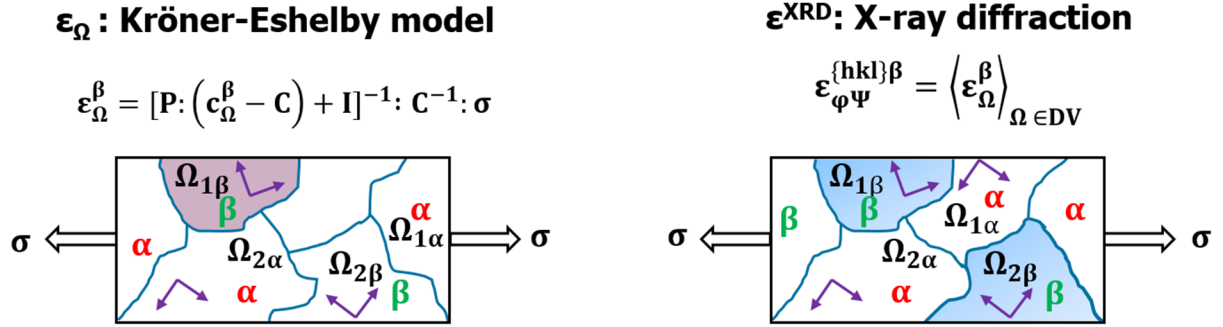


Fig. 2. The strain predicted by the KE model and the strain measured by X-ray diffraction.

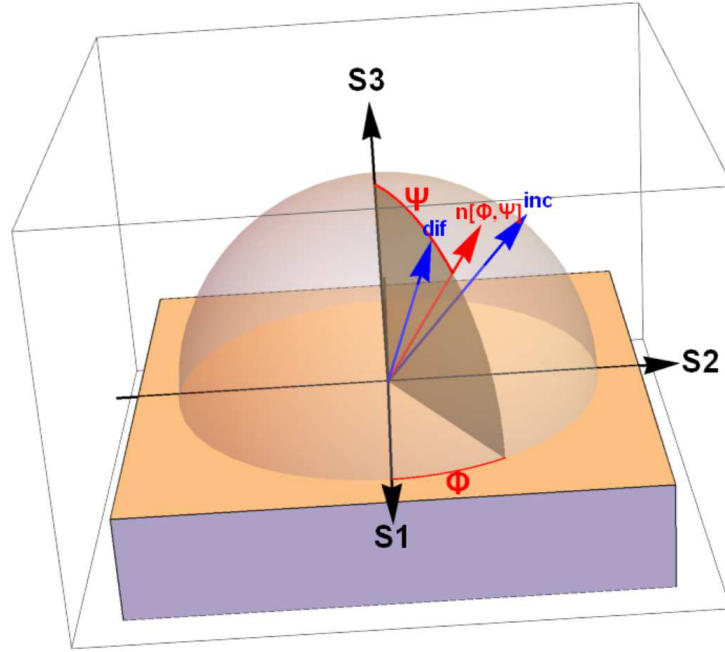


Fig. 3. Definition of the tilt and azimuth angles (Ψ and ϕ) and the scattering vector \vec{n} in the chi acquisition mode. Incident and diffracted beam are represented by blue arrows.

The SCECs of the studied phase are extracted by fitting Eqs. 14 and 16 to the macroscopic experimental quantity (measured by impulse excitation technique) and to the microscopic experimental quantity (measured by X-ray diffraction under imposed loading).

3. Experimental details

The methodology presented above will be applied in order to determine the SCECs of the W_β phase included in a two-phase tungsten thin film. This choice allows to propose a first set of values of the W_β SCECs which are not found in the literature. Then a second sample, with a different crystallographic texture was used to check the consistency of the approach by predicting the macroscopic values from the single-crystal values obtained from the first sample.

3.1. Deposition procedure

Two tungsten thin films were deposited by DC magnetron sputtering at ambient temperature. One (called sample A) will be used to determine the SCECs of the W_β phase and the other one (called specimen B) will be used for the validation.

For sample A, tungsten thin films (2.1 μm) were deposited on silicon wafers, glass and steel substrates by sputtering a tungsten target of 99.95% purity rectangular target (200*100*6

mm³) using a Plassys-MP450 reactor. For specimen B, tungsten films (2.9μm) were deposited on glass substrates by DC magnetron sputtering of 99.95% purity circular target (10 cm radius and 6 mm thickness) using an ALCATEL SCM600 reactor. The elaboration parameters are presented in Table 1.

The substrates were ultrasonically cleaned with acetone and ethanol for 10 min. Before sputtering, the deposition chamber was pumped down to 4x10⁻⁴ Pa and the substrates were sputter-cleaned using Ar⁺ plasma for 10 min. The glass and steel substrates were respectively used for the macroscopic elastic characterization by IET and for the X-ray diffraction experiments. The silicon wafers were used for the observation of film morphology by Scanning Electron Microscopy.

Table 1. Deposition parameters.

	Sample A	Sample B
Rotation speed of the substrate holder (rpm)	3	11
Substrates-target distance (cm)	8	14
Target discharge current (A)	1	1
Ar flow rate (sccm)	20	15
Deposition pressure (Pa)	0.3	0.3
Time (h)	4	5
Film thickness (μm)	2.1	2.9

3.2. Macroscopic elasticity measurements

The macroscopic elasticity constants (E_x and G_{yz}) of the deposited tungsten film was measured using IET following the same procedure explained in our previous works [33, 34].

3.3. Microstructure

The grain morphology of the deposited film was analyzed using a Hitachi S3500N SEM-FEG.

The film crystalline structure and texture were investigated by X-ray diffraction using a Bruker D8 Advance diffractometer equipped with a CuK_α ($\lambda=0.15418$ nm) tube radiation

operated at 40 kV and 40 mA. The tube was used with point focus mode and the incident beam was shaped by a 1 mm collimator.

Pole figures were acquired as follows: the azimuth angle ϕ was varied between 0° and 360° and the tilt angle ψ was varied between 0° and 60° . The diffractometric angle 2θ was varied between 0° and 150° . The step measurement on the sampling angles was defined using the equal area projection method introduced by Matthies and Wenk [31, 35]. A resolution of 10° was defined on the sampling angles.

3.4. Strain measurement

In order to analyze the microscopic elastic response of the W_β phase presented by Eq. 16, a biaxial stress state was applied to the film using a polymer template made by 3D printing. The templates have known curvature radii R (Fig. 4). Knowing the curvature radius on the longitudinal direction (x) and supposing a null curvature radius on the transverse direction (y) and a planar stress state ($\sigma_{zz}=0$), the stress and strain tensors applied to the film are expressed by:

$$\varepsilon = \begin{pmatrix} \frac{h}{2R} & 0 & 0 \\ 0 & 0 & 0 \\ 0 & 0 & \frac{-\nu}{E}(\sigma_{xx} + \sigma_{yy}) \end{pmatrix} \quad \sigma = \begin{pmatrix} \frac{hE}{2R(1-\nu^2)} & 0 & 0 \\ 0 & \nu\sigma_{xx} & 0 \\ 0 & 0 & 0 \end{pmatrix} \quad 18$$

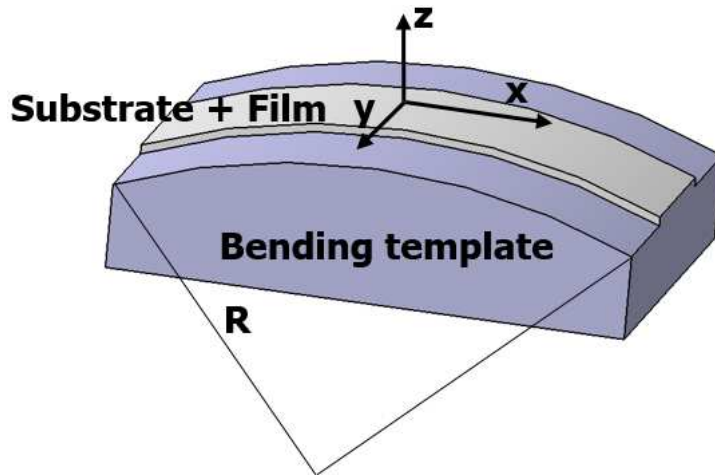


Fig. 4. The bending template.

In order to take into account the initial residual stress state of the deposited tungsten film, the variation of strains between an initial and a loaded states (Eq. 19) was considered. The lowest loaded state ($R=330$ mm) was taken as the initial state. The loading was assumed

purely elastic and thus the initial residual stress did not change during the experiment. With this approach, the stress-free lattice parameters are not necessary.

$$\Delta \varepsilon_{\text{meas}}^{(hkl, \phi \Psi)_i} = \varepsilon_{\text{R}}^{(hkl, \phi \Psi)_i} - \varepsilon_{\text{R}=330\text{mm}}^{(hkl, \phi \Psi)_i} \quad 19$$

With $\Delta \varepsilon_{\text{meas}}^{(hkl, \phi \Psi)_i}$ is a function of the SCECs to be extracted. Five bending templates with different curvature radii (330mm, 150mm, 120mm, 100mm and 80mm) were used.

4. Experimental data

4.1. Morphology

Fig. 5 shows a fractured cross sectional SEM image of the deposited tungsten film. It can be clearly seen that the film exhibits a columnar growth. This can be due to the deposition pressure and to the absence of bias. The columnar morphology leads to a low density of the film compared to the bulk material. The film porosity fraction was determined from densities using Eq. 20. The film density was calculated using its dimensions and mass. The density of the bulk tungsten used in the calculation is $\rho=19\ 250\ \text{kg/m}^3$. The obtained value for the porosity fraction of sample A is $V_p=1.7\%$.

As we can see from Fig. 5, the film is made up of needle-like grains (morphological texture) which is susceptible to induce an elastic anisotropy even in the absence of crystallographic texture [25, 36]. The morphological texture was taken into account in the mechanical modeling. The columnar shape of the grains was introduced in the KE simulation using the ratios (Morris tensor) presented in Eq. 7. The grains were considered as ellipsoidal inclusions with a radius in the direction perpendicular to the film surface six times larger than the radii in the two other directions (Fig. 6).

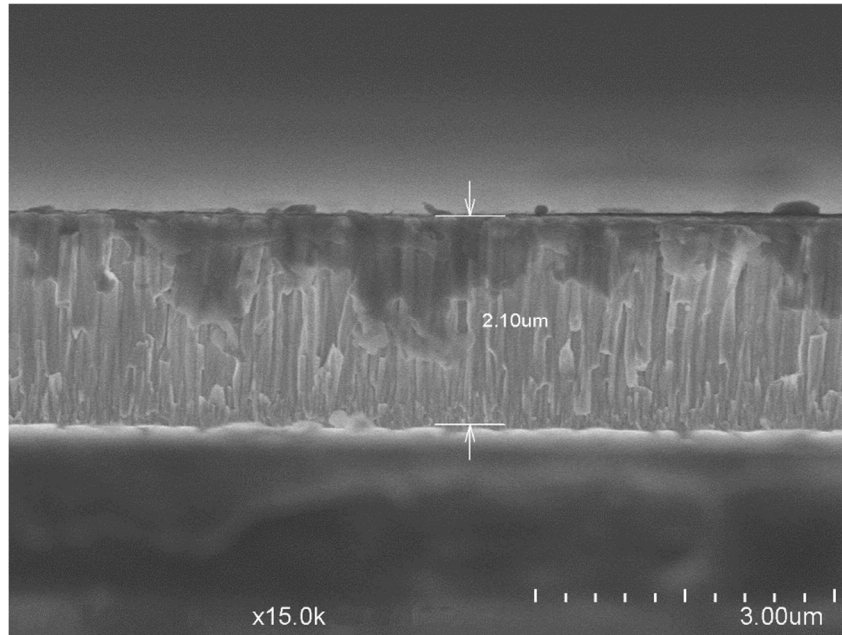


Fig. 5. Cross section SEM image of the tungsten film.

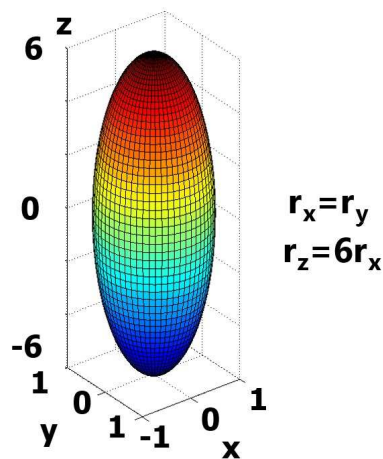


Fig. 6. Ellipsoidal grain (needle-like grain).

$$p = 1 - \frac{\text{film density}}{\text{bulk density without pores}} \quad 20$$

4.2. Structure

The identification of the tungsten film phases was performed on the sum of the diffraction patterns collected using the experimental procedure introduced in §3.3. Fig. 7 shows the sum of all the patterns for all the azimuth/tilt angles used. This diffraction pattern reveals the presence of two phases: a stable cubic body centered ($Im\text{-}3m$) W_α phase and a metastable cubic ($A15$, $Pm\text{-}3n$) W_β phase. The presence of the metastable W_β phase in tungsten films deposited by magnetron sputtering has been reported in many previous works

[34, 37-41]. Its presence may be due to the out-equilibrium character of magnetron sputtering technique. The structure of these two phases can be obtained in the Crystallography Open Database (COD: <http://www.crystallography.net>) as entries 9006486 (α phase) and 9008583 (β phase).

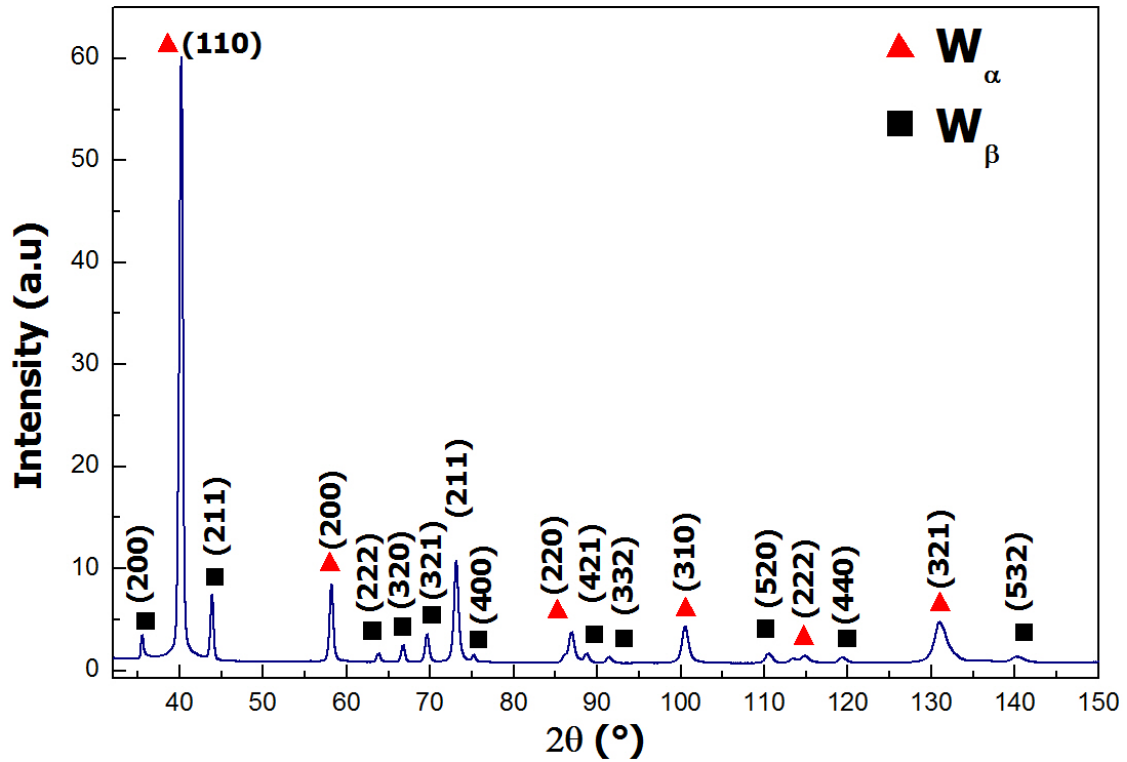


Fig. 7. Sum of the diffraction patterns of sample A.

4.3. Volume fractions of the W_α and W_β phases

The volume fractions of the two phases were calculated using MAUD software (Material Analysis Using Diffraction) [42] by simulating the experimental pattern of Fig. 7 through the Rietveld method [43]. The texture of the film was taken into account in the simulation using the standard functions in the MAUD software. The volume fractions deduced from the simulation are: $V_\alpha=74.4\%$ and $V_\beta=25.6\%$.

4.4. Texture

Figs. 8, 9, 10 and 11 show the experimental and recalculated pole figures of the W_α and W_β phases drawn with the DIFFRAC.TEXTURE software. The recalculated poles figures were calculated using the Harmonic method.

The $\{110\}_\alpha$, $\{200\}_\alpha$ and $\{211\}_\alpha$ experimental and recalculated pole figures (Figs. 8 and 9) show that the W_α phase exhibits a texture with a $\{110\}$ axis perpendicular to the film surface

and a $\langle 1\bar{1}0 \rangle$ orientation parallel to the longitudinal direction of the sample with an offset of 5° . This type of texture is often called Rotated Goss texture. We can notice that the measured intensities spread by about 10° in tilt and 40° in azimuth around the ideal Rotated Goss component. The $\{200\}_\beta$, $\{211\}_\beta$ and $\{222\}_\beta$ experimental and recalculated pole figures (Figs. 10 and 11) show that the W_β phase exhibits a texture with a $\{100\}$ axis perpendicular to the film surface and a $\langle 0\bar{1}0 \rangle$ orientation parallel to the longitudinal direction of the sample with also an offset of 5° . This type of texture can be described as a cube texture rotated by 45° . The intensity spread around the ideal component is about the same than in the case of the W_α phase, in the tilt and azimuth directions. This angular spread of the texture is usual in magnetron sputtering and can be due to the angle between the normal to the substrate surface and the coating vapour flux [44].

The relation between the sample system and the crystal system is described through a transformation matrix using the Euler angles according to the Bunge convention [45]. The orientation of each crystallite in Eqs. 1 to 16 is defined as $\Omega \equiv (\varphi_1, \Phi, \varphi_2)$.

In the mechanical modeling, the angular spread of the texture around the ideal Goss/Cube components is neglected. This allows to describe the texture of each phase using a single orientation (Crystallite Group Method). The Euler angles according to the Bunge convention used to describe the W_α and W_β textures are respectively: $\varphi_{1\alpha} = 0^\circ$, $\Phi_\alpha = 90^\circ$, $\varphi_{2\alpha} = 40^\circ$ and $\varphi_{1\beta} = 90^\circ$, $\Phi_\beta = 95^\circ$, $\varphi_{2\beta} = 90^\circ$.

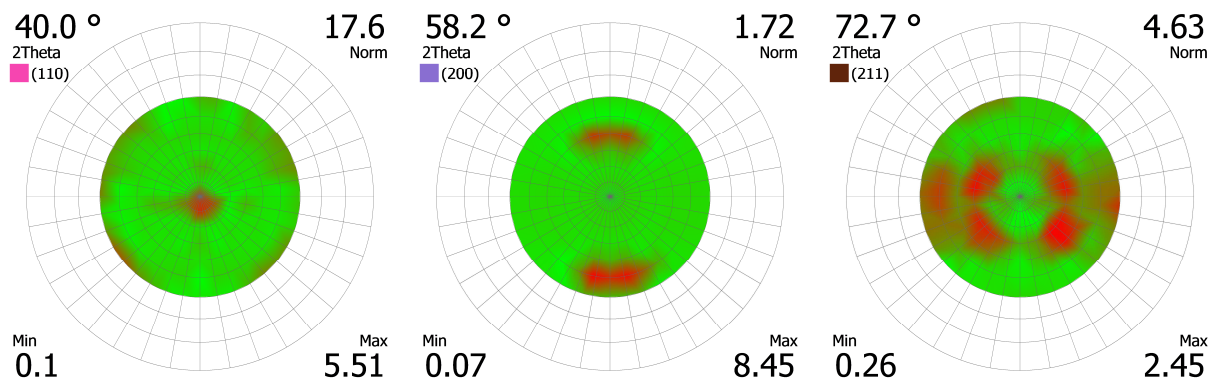


Fig. 8. $\{110\}_\alpha$, $\{200\}_\alpha$ and $\{211\}_\alpha$ experimental pole figures of the W_α phase. The pole figures are represented in stereographic projection.

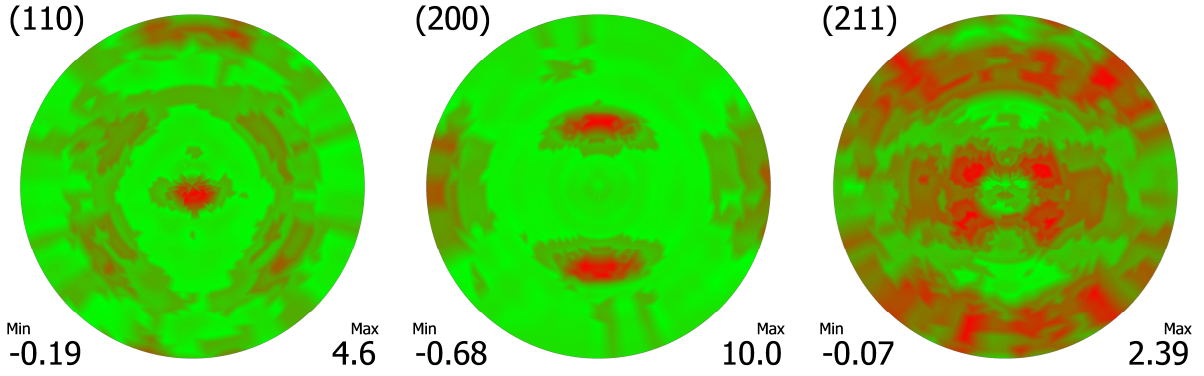


Fig. 9. $\{110\}_\alpha$, $\{200\}_\alpha$ and $\{211\}_\alpha$ recalculated pole figures of the W_α phase. The pole figures are represented in stereographic projections.

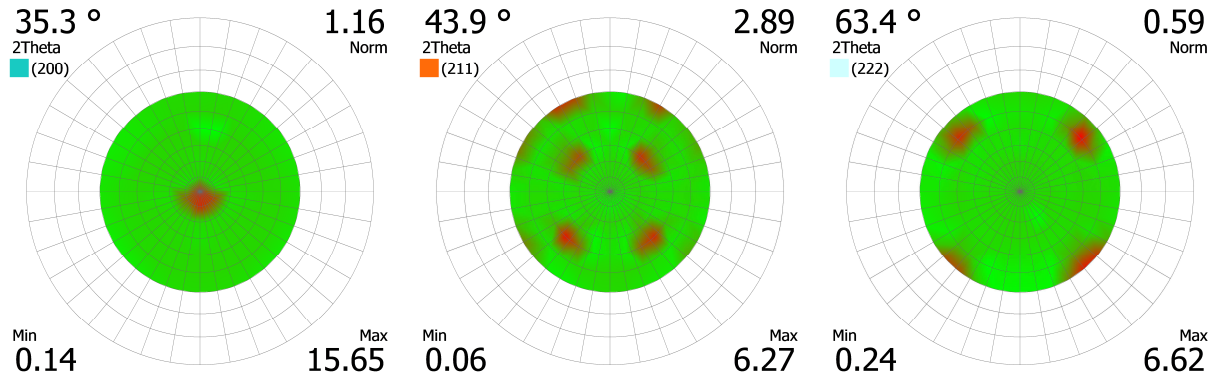


Fig. 10. $\{200\}_\beta$, $\{211\}_\beta$ and $\{222\}_\beta$ experimental pole figures of the W_β phase. The pole figures are represented in stereographic projection.

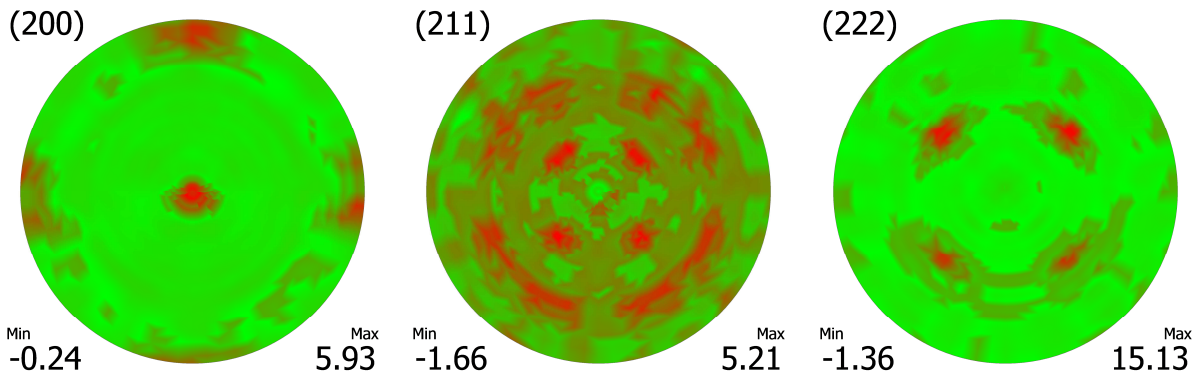


Fig. 11. $\{200\}_\beta$, $\{211\}_\beta$ and $\{222\}_\beta$ recalculated pole figures of the W_β phase. The pole figures are represented in stereographic projections.

4.5. The macroscopic elasticity constants of the film (E_x and G_{yz})

The torsional and flexural resonance frequencies of the glass substrates before and after deposition are given in Table 2. Table 3 presents the macroscopic elasticity constants of the

tungsten thin films deposited on the glass substrates and their uncertainties. The elasticity constants and their uncertainties were calculated using the methodology presented in our previous works [33, 34]. The masses and dimensions of the substrates and the films are presented in Table 4.

Table 2. Resonance frequencies of glass substrates before and after deposition of the tungsten films.

Sample	Flexural resonance frequency (Hz)		Torsional resonance frequency (Hz)	
	Before deposition	After deposition	Before deposition	After deposition
A	973.1	979.15	1801.6	1910.61
B	957.8	963.96	1772.98	1781.86

Table 3. Macroscopic elasticity constants of the deposited tungsten films. $u(x)$ represents the standard uncertainty calculated according to the GUM standard [46].

Sample	E_x (GPa)	G_{yz} (GPa)	$u(E_x)$ (GPa)	$u(G_{yz})$ (GPa)
A	329.6	123.7	4.9	1.6
B	328.6	121.8	5.1	1.5

Table 4. Masses and dimensions of the substrates and the films.

	Length (mm)	Width (mm)	Thickness (mm)	Mass (g)
Substrate of sample A	75.31	25.384	1.01	4.756
Substrate of sample B	75.316	25.392	0.9937	4.681
Film of sample A	75.31	25.384	0.0021	0.076
Film of sample B	75.316	25.392	0.0029	0.0775

B				
---	--	--	--	--

4.6. X-ray data

X-ray strain measurements were performed on two different plane families, $\{440\}_\beta$ and $\{520\}_\beta$. The experiments achieved on the $\{532\}_\beta$ family of planes were not used because of their diffraction peaks not well defined. Fig. 12 shows the $\{440\}_\beta$ and $\{520\}_\beta$ recalculated pole figures. The strain measurements were done on the intensity poles of the ideal rotated Cube component indicated by white triangles in Fig. 12. The intensity poles with a tilt angle superior to 75° were not used to avoid optical aberrations. The measurements are shown in Figs. 13 and 14. Figs. 13 and 14 show a linear relationship between the strain variation and the inverse of the curvature radius $\left(\frac{1}{R}\right)$ which indicates that the loading remains linearly elastic and that the dispersion is reasonable. It confirms that no plastic deformation occurs during solicitation and consequently no modification in the film residual stress state.

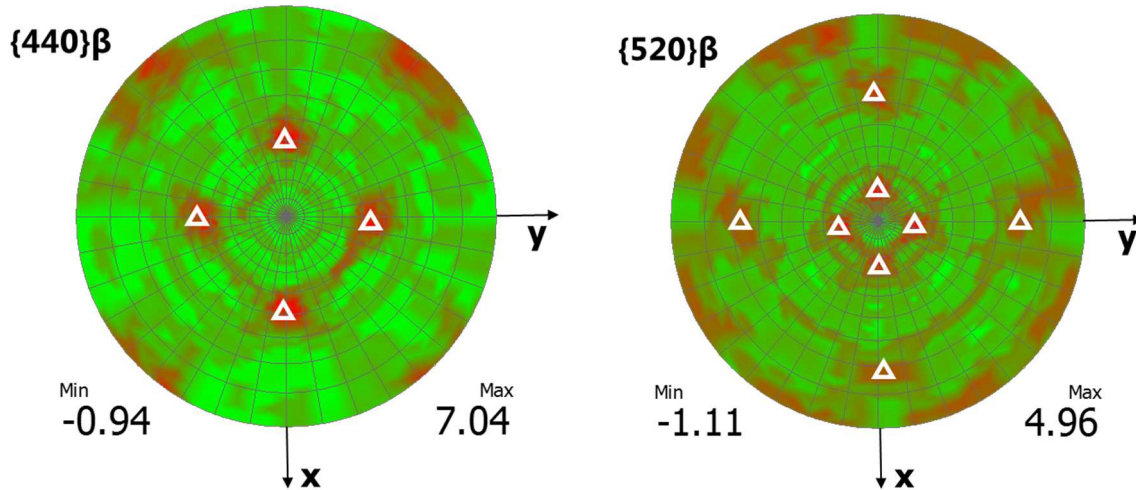


Fig. 12. $\{440\}_\beta$ and $\{520\}_\beta$ recalculated pole figures of the W_β phase. The white triangles represent the intensity poles on which the strain measurements were performed. The curvature radius is applied along the longitudinal direction (x).

5. Determination of the single-crystal elasticity constants of the W_β phase

In order to calculate the SCECs of the W_β phase, the expressions of the macroscopic elasticity constants (E_x and G_{yz}) and strain variations ($\Delta\varepsilon_{meas}^{(hkl,\phi\Psi)\beta}$) derived using the self-consistent model was fitted to the experimental data by minimizing a function defined as the difference between the experimental and simulated quantities (Eq. 21). The uncertainties of

the measured quantities were used to weight the experimental data with the inverse of their uncertainties.

$$H(\mathbf{c}_{ij}^{\beta}) = \left[\frac{E_{TEI}^{TEI} - E_{TEI}^{calc}}{u(E_{TEI})} \right]^2 + \left[\frac{G_{yz}^{TEI} - G_{yz}^{calc}}{u(G_{TEI})} \right]^2 + \sum_{i=1}^n \left[\frac{\Delta \varepsilon_{meas}^{(hkl, \phi \Psi)\beta} - \Delta \varepsilon_{calc}^{(hkl, \phi \Psi)\beta}}{u(\Delta \varepsilon_{meas}^{(hkl, \phi \Psi)\beta})} \right]^2 \quad 21$$

The SCECs of the W_{α} phase used in the calculation are the average of data found in the literature (Table 5). The Cowin and Mehrabadi convention was used for the index contraction [47]. The porosity (1.7%, §4.1) was taken into account in the calculation as a third phase and supposing its rigidity tensor equal to zero. Thus, Eq. 14 is rewritten as follow:

$$\mathbf{C} = \left[V_{\alpha} \langle \mathbf{c}_{\Omega}^{\alpha} : [\mathbf{P} : (\mathbf{c}_{\Omega}^{\alpha} - \mathbf{C}) + \mathbf{I}]^{-1} \rangle_{\Omega \in \alpha} + V_{\beta} \langle \mathbf{c}_{\Omega}^{\beta} : [\mathbf{P} : (\mathbf{c}_{\Omega}^{\beta} - \mathbf{C}) + \mathbf{I}]^{-1} \rangle_{\Omega \in \beta} + V_p \langle \mathbf{c}_{\Omega}^p : [\mathbf{P} : (\mathbf{c}_{\Omega}^p - \mathbf{C}) + \mathbf{I}]^{-1} \rangle_{\Omega \in p} \right] \quad 22$$

With zero rigidity of porosity, the third term will disappear and the volume fractions of the two phases (V_{α} and V_{β}), presented in §4.2, are weighted by the solid volume fraction ($1 - V_p$). Therefore, no particular form was attributed to the porosity.

Table 5. SCECs of the W_{α} phase.

Material	Lattice parameter (Å)	c_{11}^{α} (GPa)	c_{12}^{α} (GPa)	c_{44}^{α} (GPa)	A^{α}	Reference
W_{α}		501	198	302	0.997	[48]
W_{α}	3.183	521.1	186.3	301	0.899	[49]
W_{α}	3.190	520.9	200.2	282.2	0.88	[50]
W_{α}	3.190	518	197	282	0.878	[51]
W_{α}		553	207	356	1.029	[52]
W_{α}		529.94	211.19	278.88	0.875	[53]
W_{α}		565	316	248	0.996	[54]
Average		529.84	216.53	292.87	0.936	
Standard deviation		21.98	44.57	33.1	0.068	

The SCECs of the W_{β} phase obtained from the minimization procedure and its Zener anisotropy ratio [55] are presented in Table 6. The uncertainty presented in Table 6 was calculated using the Monte Carlo method: knowing the distribution (standard uncertainty) of input data, the distribution of SCECs can be computed by generating random sets of synthetic

data centered on the experimental values. From Table 6, we can see that the W_β phase has an anisotropic elastic behavior and is more compliant than the W_α phase.

Table 6. The SCECs constants of the W_β phase and its Zener anisotropy ratio A .

	c_{11}^β (GPa)	c_{12}^β (GPa)	c_{44}^β (GPa)	A^β
Value	350.3	108.8	180.1	0.75
uncertainty	45.6	23.6	71.8	0.2

Table 7 presents the macroscopic elasticity constants of the two-phase tungsten film calculated with the KE model using the results presented above in Table 6. A good agreement between the recalculated elasticity constants and those measured by IET is observed. The difference is lower than the uncertainty (Table 7). Figs. 13 and 14 show the variation of the strains between an initial state and a loaded state. The first loaded state ($R= 330$ mm) was taken as initial state. A good agreement between the theoretical and the experimental points corresponding to the well-defined diffraction peaks (enough of intensity and sharpness) was observed.

Table 7. Comparison between the macroscopic elasticity constants of the tungsten film calculated with the KE model using the results of Table 6 and these measured by IET.

Sample A				
Values in GPa	E_x	$u(E_x)$	G_{yz}	$u(G_{yz})$
Measured by IET	329.6	4.9	123.7	1.6
Recalculated from c_{ij}^β and KE model	341.4	12.5	124.7	7.5
Difference between recalculated and measured values	11.8		1.0	

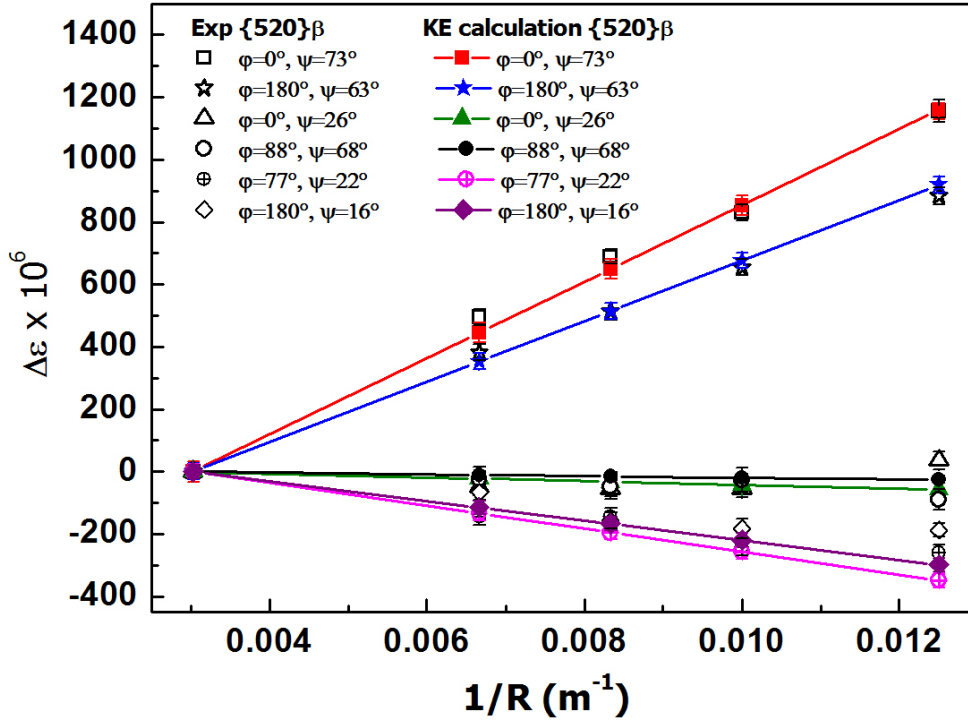


Fig. 13. Experimental and calculated values of the strain obtained by in-situ diffraction of the $\{520\}_\beta$ family of planes as a function of the inverse of the curvature radius. The theoretical points are calculated using the SCECs of the W_β phase of Table 6 and the KE model.

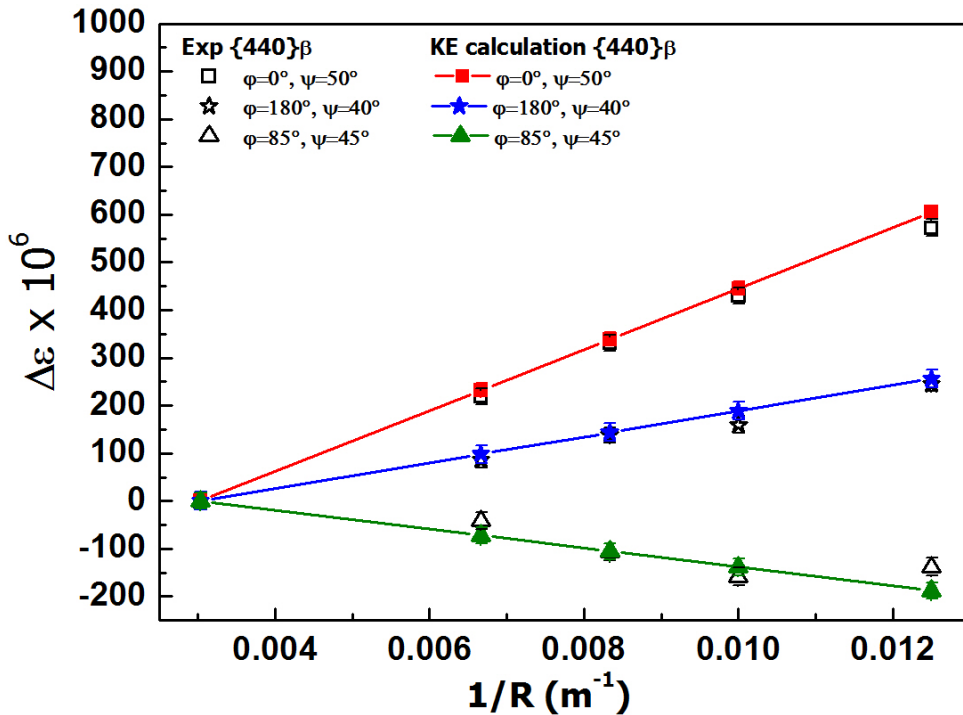


Fig. 14. Experimental and calculated values of the strain obtained by in-situ diffraction of the $\{440\}_\beta$ family of planes as a function of the inverse of the curvature radius. The theoretical points are calculated using the SCECs of the W_β phase of Table 6 and the KE model.

6. Discussion

6.1. Influence of the different factors on the macroscopic behavior

The influences of the W_β volume fraction, the porosity and the crystallographic and morphological textures on the Young's and shear moduli were taken into account in the inverse method. However, it can be interesting to study the relative strength of these factors on the elasticity characteristics (E and G) of the film. Furthermore, the quantity determined by the inverse method must have enough influence on the measured data in order to give reliable results. It is indeed easy to imagine that a very small volume fraction of the unknown phase would lead to a very poor sensitivity. To quantify this effect, the factors were varied one by one with the help of the model. A reference configuration was chosen (no texture, no porosity, no β phase, spherical crystallites) and the various factors were introduced one by one with respect to this reference. The results are presented in Table 8 and shown in Fig. 15. It can be observed that, except for the morphological texture, all the factors have a significant effect (superior to the uncertainty) on the Young's and shear moduli with a dominant effect of the W_β volume fraction. This significant effect of the W_β volume fraction allows the determination of the SCECs of the W_β by the inverse method as presented in §5. The effect of texture presented in Fig. 15 corresponds to two extreme cases (isotropic film and an ideally sharp texture). This means that, in our case, the error induced by using the crystallite group method on the texture is much smaller than the effect of texture presented in Table 8. However in order to quantify the influence of the texture of the W_β phase a comparison was done between a thin film with 75% untextured α phase and 25% untextured β phase and a thin film with 75% untextured α phase and 25% textured β phase, the texture of the β phase (§4.4) was used. The results are presented in table 9. Despite, the β phase represent only 25% of the film volume its texture has an effective influence on the macroscopic elasticity constants. From table 9 it can be noted that no elastic anisotropy is induced due to the texture of the β phase. This is specific to the cube texture of the β phase actually found on our specimens. For a different textures, such as a Goss texture for the β phase, a difference of 16 GPa in the Young's modulus in directions x and z would appear.

Table 8. Effect of the morphological and crystallographic textures, the W_β volume fraction and the porosity on the Young's and shear moduli.

	E (GPa)	G (GPa)
Reference configuration: - no texture (macro-isotropy) - no porosity	390.4	150.4

- no β phase - spherical crystallites				
Texture of α phase	E_x	E_z	G_{xy}	G_{xz}
	3.1	-13.9	-5.9	3.9
presence of 1.7% porosity	13		4.8	
presence of 25% of β phase	38.4		14.4	
elongated grains in z direction	5		1	
Uncertainty of measurements performed by IET	5		1.6	

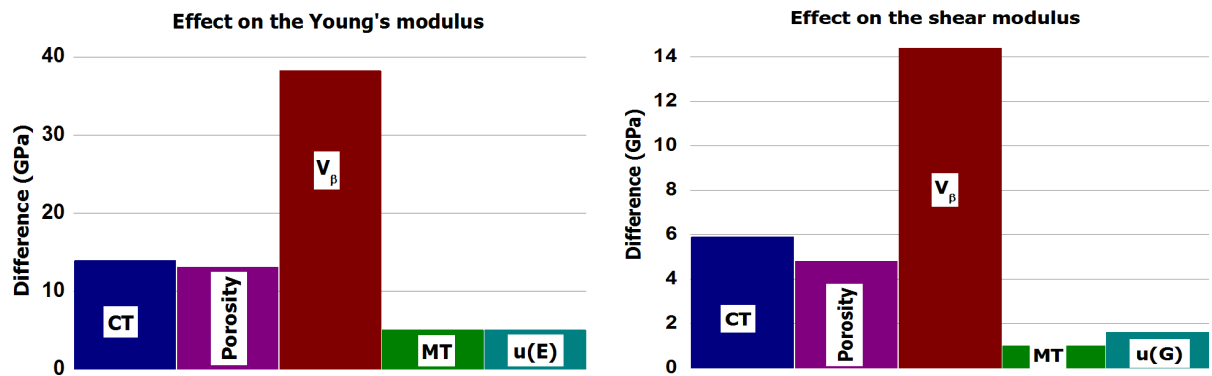


Fig. 15. Effect of the texture, the porosity and the W_{β} volume fraction on the Young's and shear moduli. (CT): Crystallographic texture, (MT): Morphological texture.

Table 9: Effect of the texture of the β phase (values in GPa).

	E_x	E_y	E_z	G_{xy}	G_{xz}	G_{yz}
75% α phase and 25% β phase (No texture)	352	352	352	136	136	136
75% non textured α phase and 25 % β phase with cube texture	365	365	365	133	133	133
Difference	12	13	15	4	3	3

6.2. Independent check on sample B

In order to check the developed methodology and the SCECs of the W_{β} tungsten phase, which to our knowledge are not known, we have used the values obtained from sample A (Table 6) to predict the macroscopic elasticity constants of sample B. The predicted elasticity constants will then be compared to those measured by IET.

Figs. 16 and 17 show respectively the recalculated pole figures of the W_α and W_β phases. It can be seen that the texture of the W_α phase can be described reasonably well by an ideal $\{110\}$ fiber and the texture of the W_β phase by an ideal $\{100\}$ fiber. The phases proportions were determined using MAUD as in §4.3. The tungsten film contains 81% of W_α phase and 19% of W_β phase. The porosity (1.5%) was taken into account in the calculations. The simulation was achieved with 5000 crystallites using the KE model.

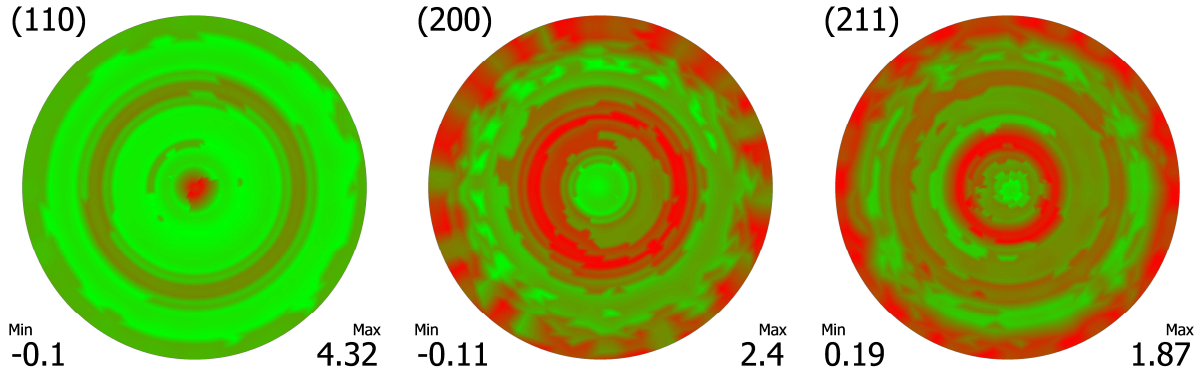


Fig. 16. $\{110\}_\alpha$, $\{200\}_\alpha$ and $\{211\}_\alpha$ recalculated pole figures of the W_α phase of sample B. The pole figures are represented in stereographic projections.

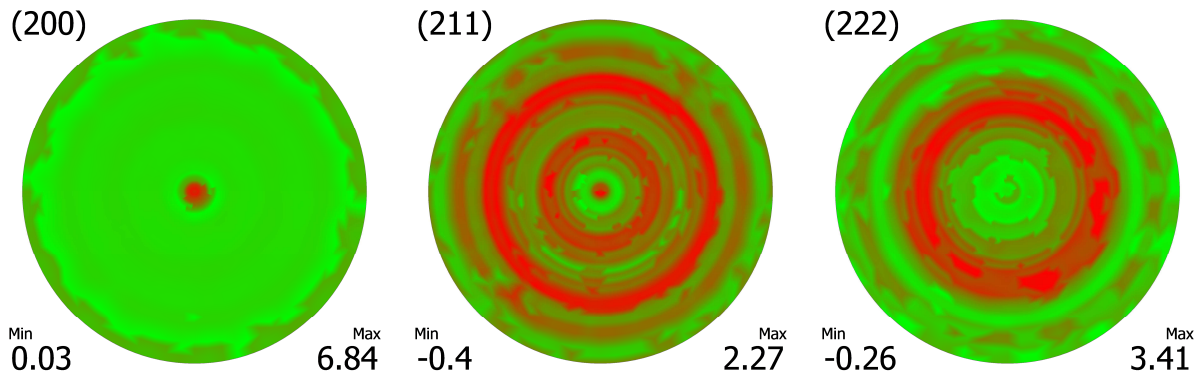


Fig. 17. $\{200\}_\beta$, $\{211\}_\beta$ and $\{222\}_\beta$ recalculated pole figures of the W_β phase of sample B. The pole figures are represented in stereographic projections.

The elasticity constants of sample B measured by impulse excitation technique and the predicted elasticity constants are presented in Table 10. A good agreement between the calculated and the measured elasticity constants can be observed and the differences can be attributed to the measurements and calculations uncertainties.

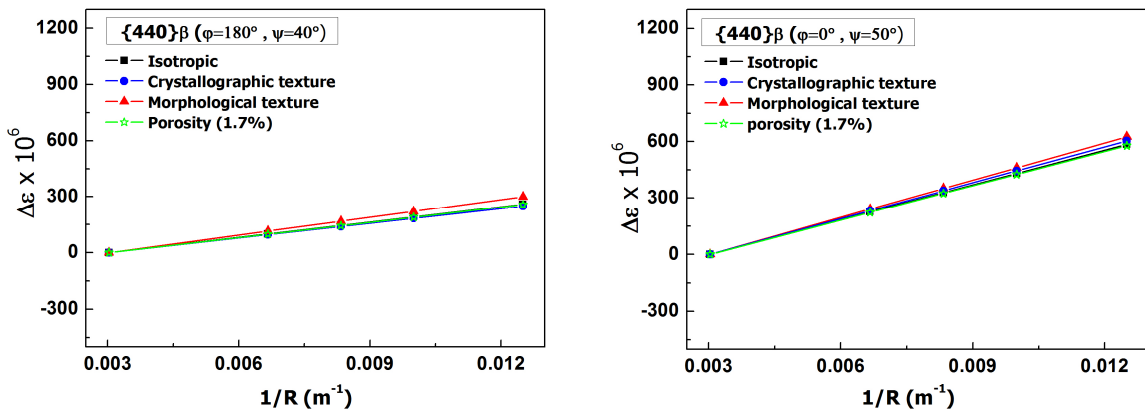
Table 10. Comparison between the macroscopic elasticity constants of the tungsten film calculated with the KE model using the results of Table 6 and these measured by IET.

Sample B				
Values in GPa	E_x	$u(E_x)$	G_{yz}	$u(G_{yz})$
Measured by IET	349.5	3.7	127.3	1.1

Recalculated from c_{ij}^β and KE model	356.1	12.5	136.5	7.5
Difference between recalculated and measured values	6.6		9.2	

6.3. Influence of the porosity, the grain shape and crystallographic texture on the behavior of the diffracting volume

As can be seen from Table 8, the effect of the morphological texture on the macroscopic elasticity constants is not very pronounced (same order of magnitude than the uncertainty). However, Koch et al. [36] and Hendrix et al. [56] have noted that the grain-shape texture has a more pronounced effect on the microscopic elastic response than on the macroscopic elastic response. In order to evaluate the effects of the morphological texture and the crystallographic texture on the behavior of the diffracting volume (observed by X-ray diffraction), a comparison of the elastic response of a textured film, a grain shape textured film and an isotropic film (no morphological texture nor crystallographic texture) was done and the results are presented in Fig. 18. As mentioned by Koch et al. and Hendrix et al., the effect of the morphological texture is more pronounced on the elastic behavior of the diffracting volume. We can see that the effects of the crystallographic texture and the grain shape texture depend on the crystallographic plane (hkl) and the measurement direction. No dominance of the crystallographic texture effect or the morphological texture effect on the microscopic behavior of the film was observed. The two effects are more or less pronounced depending on the crystallographic plane and measurement direction. The porosity effect on the elastic behavior of the diffracting volume is less important than the effects of the grain shape and the crystallographic texture.



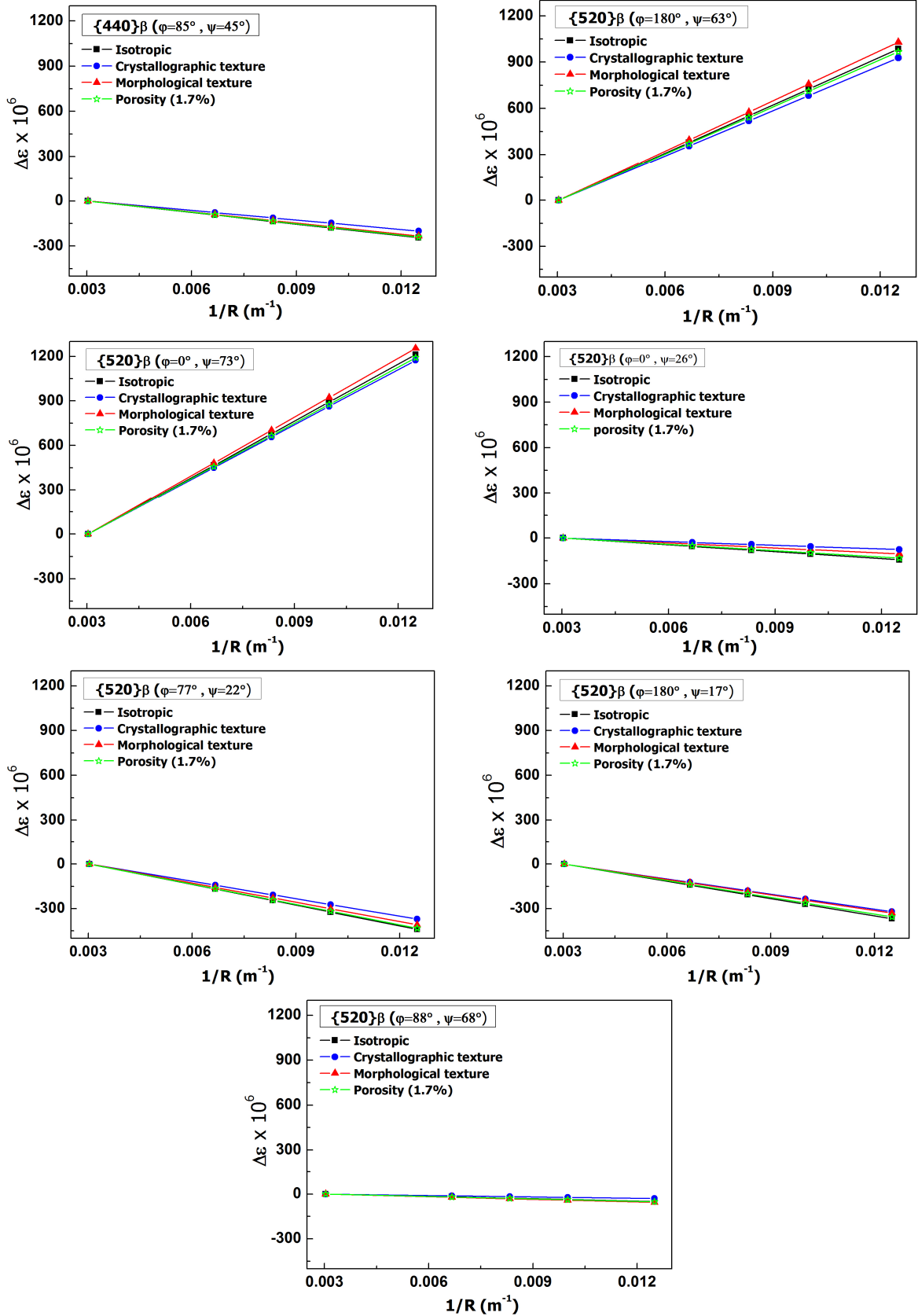


Fig. 18. Effects of the porosity and the crystallographic and the morphological textures on the elastic behavior of the diffracting volume. The strain variation was calculated using the KE model for the two-phase tungsten film. Full black squares: isotropic film. Full blue circles:

crystallographic texture (Goss/rotated cube). Full red triangles: morphological texture (as in §4.1). Green Stars: Porosity.

7. Conclusions

A methodology allowing the determination of the SCECs of a phase embedded in two-phase thin film was developed and applied to a tungsten thin film deposited by DC magnetron sputtering. The SCECs of the W_β phase, which, to our knowledge are not known, were determined. The methodology is based on the using of two experimental techniques at different scales (impulse excitation technique and X-ray diffraction) and a multiscale mechanical model (Kröner-Eshelby model). The porosity was taken into account in the mechanical modeling supposing its rigidity tensor equal to zero. The crystallographic texture was described using the crystallite group method. The morphological texture was taken into account through the Morris tensor. The analysis of uncertainty sources on the SCECs of the W_β phase showed that the total uncertainty comes mainly from the uncertainties of the experimental quantities, the measured strains, i.e. the quality of diffraction peaks and the macroscopic elasticity constants measured by IET. The uncertainties on these measurands should be improved in further studies.

To check the method, a tungsten film with a crystallographic texture different from the first one was deposited and its elasticity constants were measured by IET. Its elasticity constants were predicted using the W_β SCECs identified on the sample A. A good agreement with measurements obtained by IET was observed.

The effect of the grain-shape texture, the crystallographic texture, the porosity and the W_β volume fraction on the Young's and shear moduli of the film was studied. A significant effect of all these factors except the morphological texture was noticed and a higher contribution of the W_β volume fraction was observed. This higher contribution has a primordial role on the determination of the W_β SCECs by inverse method. As discussed on §6.1, the effect of texture presented in Fig. 15 corresponds to two extreme cases (isotropic film and a sharp texture). So the approximation made on the texture will induce a lower error. The effects of the crystallographic and morphological textures on the microscopic behavior of the film were studied. A significant effect of the two factors was observed. No domination of a one factor over the other was noticed; their contributions depend on the crystallographic plane and the measurement direction. *The porosity effect on the elastic behavior of the diffracting volume is less important than the effects of the grain shape and the crystallographic texture.*

Acknowledgments

The authors would like to thank the co-founders of CEMAV project: Région Grand Est/Champagne-Ardenne and the European Union (Fond Européen de Développement Régional).

References

- [1] V. Hauk, Structural and residual stress analysis by nondestructive methods, Elsevier, Amsterdam (1997).
- [2] K. Tanaka, M. Koiwa, Single-crystal elastic constants of intermetallic compounds, *Intermetallics* 4 (1996) S29-S39.
- [3] A. Migliori, J. D. Maynard, Implementation of a modern resonant ultrasound spectroscopy system for the measurement of the elastic moduli of small solid specimens, *Review of Scientific Instruments* 76 (2005) 121301.
- [4] R. G. Leisure, F. A. Willis, Resonant ultrasound spectroscopy, *Journal of Physics: Condensed Matter* 9 (1997) 6001-6029.
- [5] P. Sedlak, H. Seiner, M. Landa, V. Novak, P. Sittner, L. Manosa, Elastic constants of bcc austenite and 2H orthorhombic martensite in CuAlNi shape memory alloy, *Acta Materialia* 53 (2005) 3643-3661.
- [6] S. Fréour, D. Gloaguen, M. François, A. Perronnet, R. Guillén, Determination of single-crystal elasticity constants in a cubic phase within a multiphase alloy: X-ray diffraction measurements and inverse-scale transition modelling, *Journal of Applied Crystallography* 38 (2005) 30-37.
- [7] D. Faurie, P. O. Renault, E. Le Beouhris, Ph. Goudeau, Study of texture effect on elastic properties of Au thin films by X-ray diffraction and in situ tensile testing, *Acta Materialia*. 54 (2006) 4503-4513.
- [8] M. Hayakawa, S. Imai, M. Oka, Determination of single-crystal elastic constants from a cubic polycrystalline aggregate, *Journal of applied crystallography*. 18 (1985) 513-518.
- [9] T. Gnäupel-Herold, P. C. Brand, H. J. Prask, Calculation of single-crystal elastic constants for cubic crystal symmetry from powder diffraction data, *Journal of Applied Crystallography*. 31 (1998) 929-935.
- [10] C. Efstathiou, D. E. Boyce, J. S. Park, U. Lienert, P. R. Dawson, M. P. Miller, A method of measuring single-crystal elastic moduli using high-energy X-ray diffraction and a crystal-based finite element model, *Acta Materialia*. 58 (2010) 5806-5819.
- [11] C. J. Howard, E. H. Kisi, Measurement of single-crystal elastic constants by neutron diffraction from polycrystals, *Journal of Applied Crystallography*. 32 (1999) 624-633.
- [12] A. K. Singh, H. K. Mao, J. Shu, R. J. Hemley, Estimation of single-crystal elastic moduli from polycrystalline x-ray diffraction at high pressure: Application to FeO and Iron, *Physical Review Letters*. 80 (10) (1998) 2157-2160.

- [13] R. J. Talling, R. J. Dashwood, M. Jackson, S. Kuramoto, D. Dye, Determination of ($C_{11} - C_{12}$) in Ti-36Nb-2Ta-3Zr-0.3O (wt.%) (Gum metal), *Scripta Materialia*. 59 (2008) 669-672.
- [14] D. K. Patel, H. F. Al-Harbi, S. R. Kalidindi, Extracting single-crystal elastic constants from polycrystalline samples using spherical nanoindentation and orientation measurements, *Acta Materialia*. 79 (2014) 108-116.
- [15] M. Tane, K. Yamori, T. Sekino, T. Mayama, Impact of grain shape on the micromechanics-based extraction of single-crystalline elastic constants from polycrystalline samples with crystallographic texture, *Acta Materialia*. 122 (2017) 239-251.
- [16] M. Tane, H. Kimizuka, K. Hagihara, S. Suzuki, T. Mayama, T. Sekino, Y. Nagari, Effects of stacking sequence and short-range ordering of solute atoms on elastic properties of Mg-Zn-Y alloys with long-period stacking ordered, *Acta Materialia*. 96 (2015) 170-188.
- [17] M. Tane, Y. Okuda, Y. Todaka, H. Ogi, A. Nagakubo, Elastic properties of single-crystalline ω phase in titanium, *Acta Materialia*. 61 (2013) 7543-7554.
- [18] M. Tane, Y. Nagai, H. Kimizuka, K. Hahihara, Y. Kawamura, Elastic properties of an Mg-Zn-Y alloy single crystal with a long-period stacking-ordered structure, *Acta Materialia*. 61 (2013) 6338-6351.
- [19] V. Hauk, H. Kockelmann, Ermittlung der einkristallkoeffizienten aus den mechanischen und röntgenographischen elastizitätskonstanten des vielkristalls, *Z. Metallkd.* 70 (1979) 500–502.
- [20] S. Matthies, H. G. Priesmeyer, M. R. Daymond, On the diffractive determination of single-crystal elastic constants using polycrystalline samples, *Journal of Applied Crystallography*. 34 (2001) 585-601.
- [21] S. J. B. Kurz, U. Welzel, E. Bischoff, E. J. Mittemeijer, Diffraction stress analysis of highly planar-faulted, macroscopically elastically anisotropic thin films and application to tensilely loaded nanocrystalline Ni and Ni(W), *Journal of Applied Crystallography*. 47 (2014) 291-302.
- [22] M. Zaouali, J. L. Lebrun, X-ray diffraction determination of texture and internal stresses in magnetron PVD molybdenum thin films, *Surface and Coatings Technology*. 50 (1991) 5-10.
- [23] D. Faurie, P. Djemia, E. Le Bouhris, P. O. Renault, Y. Roussigné, S. M. Chérif, R. Brenner, O. Castelnau, G. Patriarche, Ph. Goudeau, Elastic anisotropy of polycrystalline Au films: Modeling and respective contributions of X-ray diffraction, nanoindentation and Brillouin light scattering, *Acta Materialia*. 58 (2010) 4998 – 5007.

- [24] D. Faurie, P. O. Renault, E. Le Bouhris, P. Goudeau, Determination of elastic constants of a fiber-textured gold thin film by combining synchrotron x-ray diffraction and in situ tensile testing, *Journal of Applied Physics*. 98 (2005) 093511.
- [25] A. Kumar, U. Welzel, E. J. Mittemeijer, Direction-dependent grain interaction in nickel and copper thin films, analysed by X-ray diffraction, *Acta Materialia*. 54 (2006) 1419-1430.
- [26] U. Welzel, S. Fréour, E. J. Mittemeijer, Direction-dependent elastic grain-interaction models – a comparative study, *Philosophical Magazine* 85 (21) (2005) 2391-2414.
- [27] U. Welzel, S. Fréour, Extension of the Vook-Witt and inverse Vook-Witt elastic grain-interaction models to general loading states, *Philosophical Magazine* 87 (26) (2007) 3921-3943.
- [28] V. E. Kröner, Berechnung der elastischen Konstanten des Vielkristalls aus den Konstanten des Einkristalls, *Zeitschrift für Physik*. 151 (1958) 504-518.
- [29] J. D. Eshelby, The determination of the elastic field of an ellipsoidal inclusion, and related problems, *Proceedings of the Royal Society A*. 241 (1957) 376-396.
- [30] P. R. Morris, Elastic constants of polycrystals, *International Journal of Engineering Science*. 8 (1970) 49-61.
- [31] U. F. Kocks, C. N. Tome, H. R. Wenk, *Texture and anisotropy: Preferred orientations in polycrystals and their effect on materials properties*, Cambridge University Press (1998).
- [32] M. François, Unified description for the geometry of X-ray stress analysis: proposal for a consistent approach, *Journal of Applied Crystallography*. 41 (2008) 44-55.
- [33] M. F. Slim, A. Alhussein, A. Billard, F. Sanchette, M. François, On the determination of Young's modulus of thin film with Impulse Excitation Technique, *Journal of Materials Research*. 32 (2017) 497-511.
- [34] M. F. Slim, A. Alhussein, F. Sanchette, B. Guelorget, M. François, An enhanced formulation to determine Young's and shear modulus of thin films by means of Impulse Excitation Technique, *Thin Solid Films*. 631 (2017) 172-179.
- [35] S. Matthies, H. R. Wenk, Optimisation of texture measurements by pole figure coverage with hexagonal grids, *Physica Status Solidi (a)*. 133 (1992) 253-257.
- [36] N. Koch, U. Welzel, H. Wern, E. J. Mittemeijer, Mechanical elastic constants and diffraction stress factors of macroscopically elastically anisotropic polycrystals: the effect of grain-shape (morphological) texture, *Philosophical Magazine*. 84 (33) (2004) 3547-3570.

- [37] Y. G. Shen, Y. W. Mai, Q. C. Zhang, D. R. McKenzie, W. D. McFall, W. E. McBride, Residual stress, microstructure, and structure of tungsten thin films deposited by magnetron sputtering, *J. Appl. Phys.* 87 (2000) 177.
- [38] B. Girault, D. Eyidi, P. Goudeau, T. Sauvage, P. Guerin, E. Le Bourhis, P. O. Renault, Controlled nanostructuring of polycrystalline tungsten thin films, *J. Appl. Phys.* 113 (2013) 174310.
- [39] S. Djaziri, P. O. Renault, E. Le Bouhris, Ph. Goudeau, D. Faurie, G. Geandier, C. Mocuta, D. Thiaudière, Comparative study of the mechanical properties of nanostructured thin films on stretchable substrates, *J. Appl. Phys.* 116 (2014) 093504.
- [40] P. Villain, P. Goudeau, J. Ligot, S. Benayoun, K. F. Badawi, J.-J. Hantzpergue, X-ray diffraction study of residual stresses and microstructure in tungsten thin films sputter deposited on polyimide, *J. Vac. Sci. Technol. A* 21 (2003) 967.
- [41] K. Salamon, O. Milat, N. Radic, P. Dubcek, M. Jercinovic, S. Bernstorff, Structure and morphology of magnetron W films studied by X-ray methods, *J. Phys. D: Appl. Phys.* 46 (2013) 095304.
- [42] L. Lutterotti, S. Matthies and H. -R. Wenk, MAUD (Material Analysis Using Diffraction): a user friendly Java program for Rietveld Texture Analysis and more, *Proceeding of the 12th International Conference on Textures of Materials (ICOTOM-12)*, 1, 1599, (1999).
- [43] H. M. Rietveld, A profile refinement method for nuclear and magnetic structures, *Journal of Applied Crystallography.* 2 (1969) 65-71.
- [44] Y. H. Sohn, R. R. Biederman, R. D. Sisson JR, Microstructural development in physical vapour-deposited partially stabilized zirconia thermal barrier coatings, *Thin Solid Films.* 250 (1994) 1-7.
- [45] H. J. Bunge, *Texture analysis in materials science*, Butterworths, London (1982).
- [46] JCGM 100:2008(E): Evaluation of measurement data—Guide to the expression of uncertainty in measurement (2008).
- [47] M. M. Mehrabadi, S. C. Cowin, Eigentensors of linear anisotropic elastic materials, *Quarterly Journal of Mechanics and Applied Mathematics.* 43 (1990) 15-41.
- [48] M. Nakamura, S. Matsumoto, T. Hirano, Elastic constants of MoSi₂ and WSi₂ single crystals, *Journal of materials science.* 25 (1990) 3309-3313.
- [49] N. Wei, T. Jia, X. Zhang, T. Liu, Z. Zeng, X. Y. Yang, First-principles study of the phase stability and the mechanical properties of *W – Ta* and *W – Re* alloys, *AIP Advances.* 4 (2014) 057103.

- [50] X. Li, S. Schönecker, R. Li, X. Li, Y. Wang, J. Zhao, B. Johansson, L. Vitos, Ab initio calculations of mechanical properties of bcc $W - Re - Os$ random alloys: effects of transmutation of W, *Journal of Physics: Condensed Matter*. 28 (2016) 295501.
- [51] G. D. Samolyuk, Y. N. Osetsky, R. E. Stoller, The influence of transition metal solutes on the dislocation core structure and values of the Peierls stress and barrier in tungsten, *Journal of Physics: Condensed Matter*. 25 (2013) 025403.
- [52] P. Söderlind, O. Eriksson, J. M. Wills, A. M. Boring, Theory of elastic constants of cubic transition metals and alloys, *Physical Review B*. 48 (1993) 5844-5851.
- [53] D. Y. Jiang, C. Y. Ouyang, S. Q. Liu, Mechanical properties of W-Ti alloys from first-principles calculations, *Fusion Engineering and Design*. 106 (2016) 34-39.
- [54] P. Villain, Ph. Goudeau, P.-O. Renault, and K. F. Badawi, Size effect on intragranular elastic constants in thin tungsten films, *Applied Physics Letters*. 81 (2002) 4365.
- [55] C. Zener, *Elasticity and anelasticity of metals*, University of Chicago Press (1948).
- [56] B. C. Hendrix, L. G. Yu, Self-consistent elastic properties for transversely isotropic polycrystals, *Acta Materialia*. 46 (1998) 127-135.

Graphical Abstract

Schematic representation of the methodology used in the determination of the single-crystal elasticity constants

